Mon. Not. R. Astron. Soc. **000**, 000–000 (0000) Printed 13 August 2012 (MN LATEX style file v2.2)

The Origin of Disks and Spheroids in Simulated Galaxies

Laura V. Sales[1], Julio F. Navarro[2], Tom Theuns[3,4], Joop Schaye[5], Simon D. M. White[1], Carlos S. Frenk[3], Robert A. Crain[5] and Claudio Dalla Vecchia[6]

[1] *Max Planck Institute for Astrophysics, Karl-Schwarzschild-Strasse 1, 85740 Garching, Germany*
[2] *Department of Physics and Astronomy, University of Victoria, Victoria, BC V8P 5C2, Canada*
[3] *Institute for Computational Cosmology, Department of Physics, University of Durham, South Road, Durham, DH1 3LE, UK*
[4] *Department of Physics, University of Antwerp, Campus Groenenborger, Groenenborgerlaan 171, B-2020 Antwerp, Belgium*
[5] *Leiden Observatory, Leiden University, PO Box 9513, 2300 RA Leiden, Netherlands*
[6] *Max Planck Institute for Extraterrestrial Physics, Giessenbachstrae 1, 85748 Garching, Germany*

arXiv:1112.2220v2 [astro-ph.CO] 10 Aug 2012

13 August 2012

ABSTRACT

The major morphological features of a galaxy are thought to be determined by the assembly history and net spin of its surrounding dark halo. In the simplest scenario, disk galaxies form predominantly in halos with high angular momentum and quiet recent assembly history, whereas spheroids are the slowly-rotating remnants of repeated merging events. We explore these assumptions using one hundred systems with halo masses similar to that of the Milky Way, identified in a series of cosmological gasdynamical simulations: the Galaxies - Intergalactic Medium Calculation (GIMIC). At $z = 0$, the simulated galaxies exhibit a wide variety of morphologies, from dispersion-dominated spheroids to pure disk galaxies. Surprisingly, these morphological features are very poorly correlated with their halo properties: disks form in halos with high and low net spin, and mergers play a negligible role in the formation of spheroids, whose stars form primarily in-situ. With hindsight, this weak correlation between halo and galaxy properties is unsurprising given that a minority of the available baryons ($\sim 40\%$) end up in galaxies. More important to morphology is the *coherent alignment of the angular momentum* of baryons that accrete over time to form a galaxy. Spheroids tend to form when the spin of newly-accreted gas is misaligned with that of the extant galaxy, leading to the episodic formation of stars with different kinematics that cancel out the net rotation of the system. Disks, on the other hand, form out of gas that flows in with similar angular momentum to that of earlier-accreted material. Gas accretion from a hot corona thus favours disk formation, whereas gas that flows "cold", often along separate, misaligned filaments, favours the formation of spheroids. In this scenario, many spheroids consist of the superposition of stellar components with distinct kinematics, age, and metallicity, an arrangement that might survive to the present day given the paucity of major mergers. Since angular momentum is acquired largely at turnaround, morphology depends on the early interplay between the tidal field and the shape of the material destined to form a galaxy.

Key words: Galaxy: disk – Galaxy: formation – Galaxy: kinematics and dynamics – Galaxy: structure

1 INTRODUCTION

Galaxies exhibit a wide variety of morphologies, from spheroids to disks to bars to peculiar galaxies of irregular shape. Many physical properties, such as gas content, average stellar age, and the rate of current star formation, are known to correlate with morphology. Of such properties, the one that seems most tractable from a theoretical perspective is the relative importance of organized rotation in the structure of a galaxy. This is commonly referred to as the disk-to-spheroid ratio, since stellar disks are predominantly rotationally-flattened structures whereas spheroids have shapes largely supported by velocity dispersion.

Since Hubble (1926) published his original morphological classification scheme, our understanding of the provenance of these two defining features of galaxy morphology has been constantly evolving. Spheroids were once thought to originate in the swift transformation of an early-collapsing, non-rotating cloud of gas into stars (Eggen et al. 1962; Partridge & Peebles 1967; Larson 1974), whereas disks were envisioned to result from the collapse of clouds with high angular momentum and inefficient star formation

© 0000 RAS

(Eggen et al. 1962; Larson 1976). The role of mergers as a possible transformational mechanism was championed by Toomre (1977) and gained momentum as the hierarchical nature of structure (and hence, galaxy) formation became accepted (White & Rees 1978; Frenk et al. 1985).

Further development of these ideas led to a broad consensus where disks are thought to form at the center of dark matter halos as a consequence of angular momentum conservation during the dissipational collapse of gas (Fall & Efstathiou 1980; Mo et al. 1998), whereas spheroids result predominantly from merger events (see, e.g., Cole et al. 2000, and references therein). Morphology is thus a transient feature of the hierarchical formation of a galaxy: a disk galaxy may be transformed into a spheroidal one after a major merger, but could then re-form a disk through further gas accretion only to be later disrupted again by another merger. Early galaxy formation simulations gave a visually-compelling demonstration of this scenario, galvanizing support for it (see, e.g., Steinmetz & Navarro 2002).

This consensus view has been broadly implemented in semi-analytic models of galaxy formation, where the properties of galaxies are deduced directly from the physical properties and assembly history of their surrounding halos (see, e.g., Croton et al. 2006; Bower et al. 2006; Somerville et al. 2008). For example, most models assume that the specific angular momentum of galaxies and halos are similar, and that the merger history of the halos dictates that of the central galaxy.

Recent developments, however, have led to revisiting some of the assumptions of the simple scenario outlined above. For example, it has become clear that major mergers are rare, and therefore probably not the primary formation mechanism of bulges and ellipticals. Instead, "disk instabilities" (Efstathiou et al. 1982; Christodoulou et al. 1995; Mo et al. 1998), as well as repeated minor encounters, are now claimed to be the main formation path of spheroids (e.g., Parry et al. 2009; Hopkins et al. 2010; De Lucia et al. 2011; Bournaud et al. 2011). This has helped to alleviate some tension between the observed evolution of the early-type galaxy population and the major-merger rates predicted by theory (Bundy et al. 2007; Oesch et al. 2010). However, questions might remain open, as the estimation of merger times from observations is non-trivial (Lotz et al. 2011).

Further scrutiny has come from direct simulation of hierarchical galaxy formation. Conserving enough angular momentum during the hierarchical assembly of a galaxy to form a realistic stellar disk has been challenging (see, e.g., Navarro et al. 1995; Navarro & Steinmetz 1997), as has been pinning down the effect on morphology of repeated merging, especially between gas-rich galaxies (see, e.g., Robertson et al. 2006; Governato et al. 2009).

The inclusion of energetic feedback, needed to prevent the formation of too many faint or overly massive galaxies, has added an extra level of complexity to the problem, with a number of studies showing that morphologies can be radically altered when even modest changes in the strength of feedback or its implementation are introduced (Okamoto et al. 2005; Scannapieco et al. 2008; Ceverino & Klypin 2009; Sales et al. 2010; Agertz et al. 2011; Brook et al. 2011; Piontek & Steinmetz 2011). Moreover, the density threshold assumed for star formation also changes the coupling between the stellar winds and the surrounding gas, playing also a major role on the properties of simulated galaxies(Guedes et al. 2011).

More recently, the *mode* of gas accretion has been recognized as playing a potentially crucial role in galaxy morphology. Gas can flow to galaxies largely unimpeded by shocks (White & Frenk 1991) and may be collimated by the filamentary structure of the cosmic web, especially in low-mass systems and at high redshift (Kereš et al. 2005; Dekel & Birnboim 2006; van de Voort et al. 2011). This complex accretion geometry has been hypothesized to promote the formation of disks by feeding high angular momentum material directly to forming galaxies (see, e.g., Dekel et al. 2009; Brooks et al. 2009).

Further theoretical progress demands increased sophistication in numerical and semi-analytic modeling. From the simulation perspective, most studies have focussed on individual systems picked according to what the authors believe would facilitate the formation of a galaxy of predetermined morphology; for example, a recent major merger to study ellipticals (e.g., Meza et al. 2003) or a quiet, rapidly-rotating halo to study spirals (e.g., Abadi et al. 2003; Governato et al. 2007). Note that this presupposes the morphology of the resulting galaxy, and often results in the tuning of star formation and feedback parameters until, unhelpfully, results match prejudice.

Statistically-significant samples of galaxies selected in an unbiased way and simulated at high resolution are needed for new insights, a goal that, despite valiant efforts (Croft et al. 2009; Sales et al. 2009, 2010), has so far proved beyond reach of even the fastest computers and best algorithms. The situation, however, is starting to change, with the advent of simulations of volumes large enough to include dozens of well-resolved $\sim L_\star$ galaxies (Crain et al. 2009; Schaye et al. 2010; Hahn et al. 2010; Cen & Chisari 2011; Vogelsberger et al. 2011).

We explore these issues here using the GIMIC gasdynamical simulation series (Crain et al. 2009). GIMIC targeted several carefully selected regions from the Millennium Simulation (Springel et al. 2005) in an attempt to maximize the resolution of individual galaxy systems while at the same time sampling a cosmologically-significant volume. The first analyses of $z = 0$ GIMIC galaxies (Crain et al. 2010; Font et al. 2011; McCarthy et al. 2011) show that they are fairly realistic, so we feel confident that we can use them to gain insight into the origin of galaxy morphology.

This paper is organized as follows. In Sec. 2 we present briefly the numerical method and simulations. We analyze the morphologies of simulated galaxies and their origin in Secs. 3 and 4, respectively. We summarize our main conclusions in Sec. 5

2 NUMERICAL SIMULATIONS

The "Galaxies-Intergalactic Medium Interaction Calculation", (GIMIC; Crain et al. 2009), simulation series follows the evolution of five nearly spherical regions of radius $\sim 20\,h^{-1}$ Mpc each, selected from the *Millennium Simulation* (Springel et al. 2005). These regions were selected to sample environments of different density, deviating by $(-2, -1, 0, +1, +2)\sigma$ from the cosmic average, respectively, where σ is the *rms* mass fluctuation on $20\,h^{-1}\mathrm{Mpc}$ scales. The regions are spherical at $z = 1.5$, and are simulated using the standard zoom-in technique described in detail by, e.g., Power et al. (2003). We provide here a basic summary of the main characteristics of the GIMIC project, and refer the interested reader to Crain et al. (2009) for a more comprehensive description.

GIMIC uses a modified version of GADGET-3, a development of the GADGET-2 code (Springel 2005) that includes new modules to treat radiative cooling, star formation, chemical enrichment, and energetic feedback. Radiative cooling is implemented

on an element-by-element basis and thus cooling rates evolve self-consistently as a function of redshift, gas density, temperature and chemical composition (Wiersma et al. 2009). The runs also include a uniform ionizing background (Haardt & Madau 2001), with hydrogen- and helium-reionization redshifts of $z = 9$ and $z = 3.5$, respectively.

Cold gas with densities exceeding $n_H = 0.1$ cm^{-3} becomes eligible for star formation and is assumed to follow an effective equation of state, $P \propto \rho^{4/3}$, in order to minimize numerical artifacts in poorly-resolved regions (Schaye & Dalla Vecchia 2008). Stars are assumed to follow a Chabrier IMF (Chabrier 2003), and to form at a rate that depends on the local gas pressure and that matches the Kennicutt-Schmidt law (Kennicutt 1989, 1998).

Chemical enrichment is modeled as described by Wiersma et al. (2009), and tracks the synthesis of 11 individual elements. As massive stars explode as supernova (SN), they inject energy and metals into their surroundings. This feedback is implemented, in practice, by using a fraction f_{SN} of the energy released by SN in order to modify the velocity of a few (η_w) neighboring gas particles by introducing a velocity "kick" of magnitude V_w to each (Dalla Vecchia & Schaye 2008). These parameters are set in GIMIC to $f_{SN} = 0.8$, $\eta_w = 4$ and $V_w = 600$ km/s, which results in a good match to the peak of the global star formation rate density (Crain et al. 2009; Schaye et al. 2010).

All GIMIC runs adopt the same cosmological parameters as the original *Millennium Simulation*, which were chosen to be consistent with the WMAP-1 constraints: $\Omega_m = 0.25$; $\Omega_\Lambda = 0.75$; $\Omega_b = 0.045$; $n_s = 1$; $\sigma_8 = 0.9$; $H_0 = 100\,h$ km s^{-1} Mpc^{-1}; $h = 0.73$.

The particle mass in the simulations is $1.4 \times 10^6\,h^{-1}\,M_\odot$ and $6.6 \times 10^6\,h^{-1}\,M_\odot$ for the baryons and dark matter, respectively. The gravitational softening is initially fixed in comoving units, but is fixed at $z = 3$ and thereafter to $\epsilon = 0.5\,h^{-1}$ kpc (Plummer equivalent) in physical units. We shall focus here on the two GIMIC regions that have been run to $z = 0$ at this resolution: the -2σ and 0σ. As we discuss below, aside from the expected difference in the number of systems of given mass, we see no systematic dependence of our results on the overdensity of the region, which may therefore be thought to apply to average regions of the Universe.

We have used SUBFIND (Springel et al. 2001; Dolag et al. 2009) to identify galaxies in the high-resolution regions of the GIMIC runs. We shall only consider in the analysis the *central* galaxies of halos within a narrow range of virial[1] mass: $0.5 < M_{200}/10^{12}\,h^{-1}\,M_\odot < 1.5$. This ensures homogeneity in the set of systems selected for analysis and eliminates complications that may arise from considering satellites of larger systems. At redshift $z = 0$, these criteria identify 38 and 62 galaxies in the -2σ and 0σ runs, respectively. Each of these halos is resolved with roughly 200,000 particles (dark plus baryonic), allowing for a reasonable estimate of the relative importance of the disk and spheroidal components. None of the results we discuss here show significant dependence on which region we consider, so we will group the 100 galaxies together without making distinction regarding the GIMIC run where they were identified.

[1] Virial quantities throughout this paper are defined at the radius enclosing 200 times the critical density for closure.

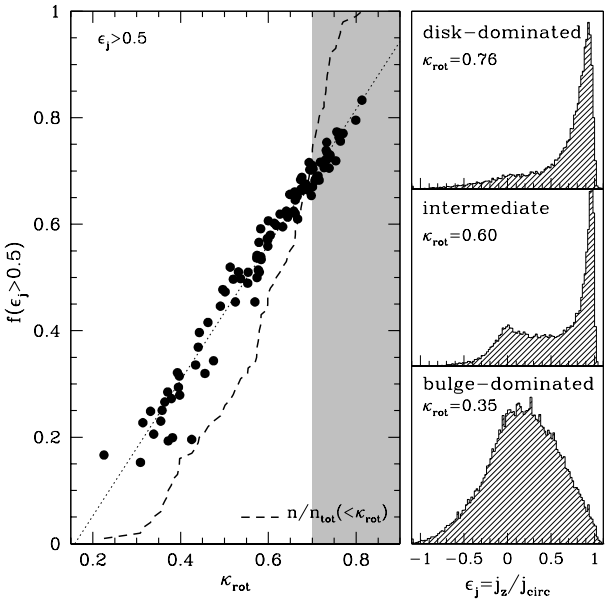

Figure 1. *Left:* The kinematic morphology parameter, $\kappa_{\rm rot}$, defined as the fraction of kinetic energy in organized rotation (eq. 1), versus the fraction of stars with circularity parameter $\epsilon_j > 0.5$. The cumulative fraction is shown with a dashed line. The shaded region ($\kappa_{\rm rot} > 0.7$) indicates where "disk dominated" galaxies lie in this plot. *Right:* The distribution of circularities, $\epsilon_j = j_z/j_{\rm circ}(E)$, is shown for three galaxies with different values of $\kappa_{\rm rot}$.

3 SIMULATED GALAXY MORPHOLOGIES

3.1 Morphology estimates

As discussed in Sec. 1, we shall adopt a somewhat narrow definition of morphology based on the importance of ordered rotation in the structure of a galaxy. Although we refer to this as the ratio of disk to spheroid, it should be noted that this may differ, at times substantially, from traditional bulge-to-disk decompositions based on photometric data. The latter are based on assumptions regarding the shape of the brightness profile of disks, usually assumed to be exponential, and spheroids, assumed to follow either de Vaucouleurs or Sersic profiles. As discussed by Abadi et al. (2003) (see also Scannapieco et al. 2010), these assumptions are only weakly fulfilled by simulated galaxies, and kinematic decompositions can give rather different spheroid-to-disk ratios than photometric ones. Photometric studies can also be affected by color gradients, extinction, and projection effects (see, e.g., Governato et al. 2009). We avoid these complications by focusing our analysis on kinematic data alone, although we plan to consider the implications of our results for photometric studies in future work.

The importance of ordered rotation may be clearly appreciated from the distribution of the stellar orbital *circularity* parameter, $\epsilon_j = j_z/j_{\rm circ}(E)$, defined as the ratio of the component of the specific angular momentum perpendicular to the disk (i.e., aligned with the total angular momentum of the galaxy), j_z, to that of a circular orbit with the same binding energy, $j_{\rm circ}(E)$. Defined in this way, ϵ_j takes values in the range $(-1,1)$, where the extreme values correspond to the counter- and co-rotating circular orbits in the symmetry plane of the galaxy, respectively.

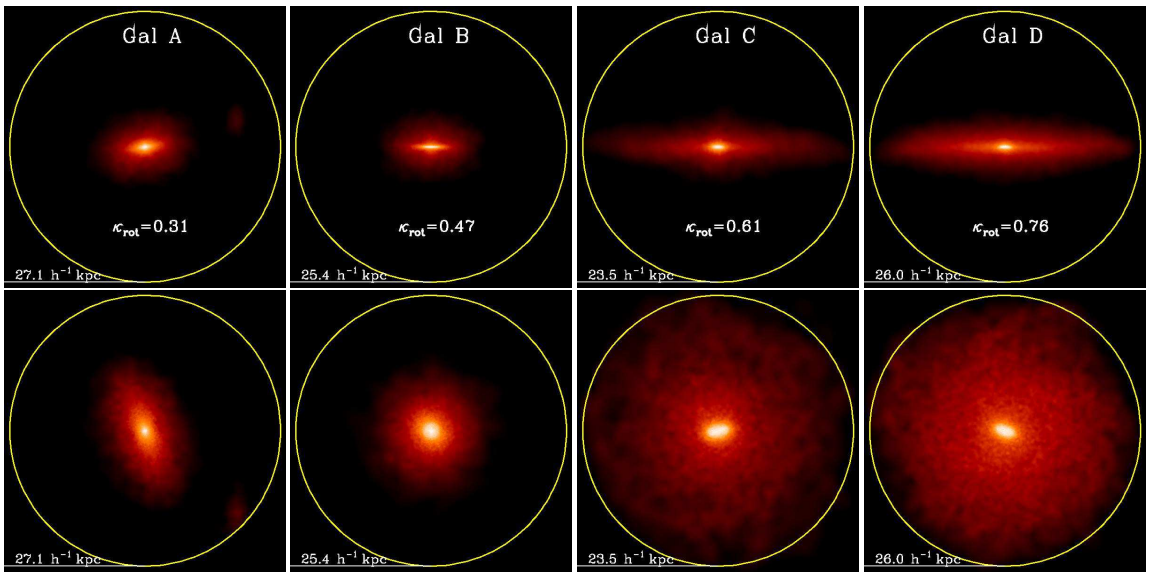

Figure 2. Illustration of the structure of four galaxies in our sample with increasing degree of rotational support (left to right). The first and second rows show edge-on and face-on projections of the stellar distribution. The yellow circle marks the radius, $r_{\rm gal} = 0.15\, r_{200}$, used to define the galaxy.

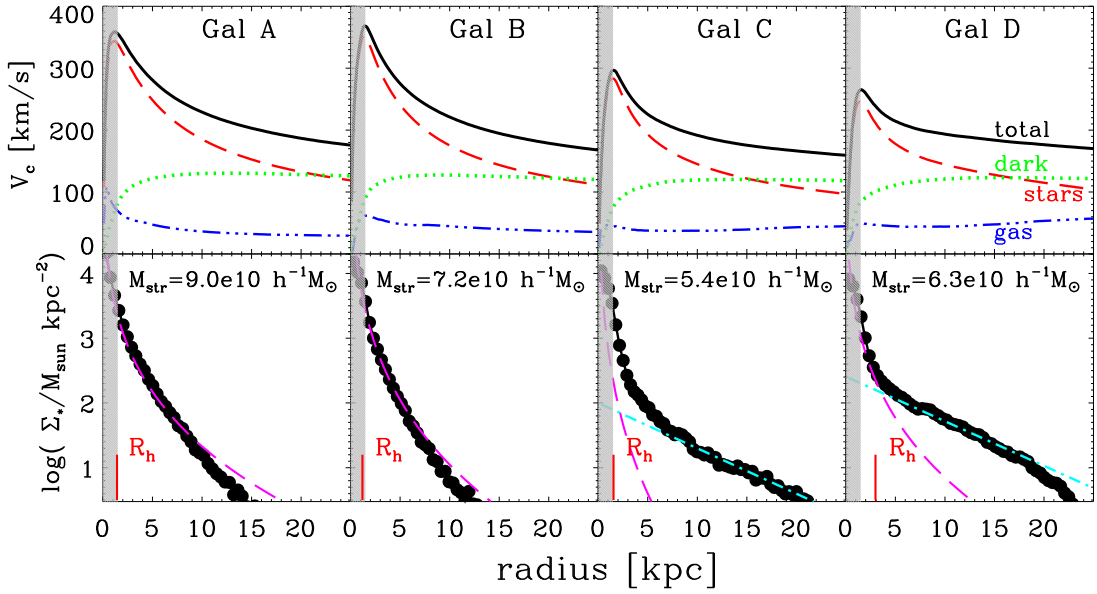

Figure 3. Top and bottom rows show the circular velocity profile, $V_c(r)$, and the stellar surface density profiles, respectively, of galaxies A-D in Fig. 2. Red lines in the bottom panels indicate the stellar half-mass radius of each galaxy. Dashed magenta lines indicate de Vaucouleurs' $R^{1/4}$ profile fits. Straight dashed lines in blue indicate exponential profile fits. The shaded area highlights a radius equal to three Plummer-equivalent gravitational softening scalelengths. Note that spheroids can be well fit by a single $R^{1/4}$ law, but that disk-dominated galaxies show evidence of a de Vaucouleurs' spheroid plus an exponential disk. Disks are extended and have approximately flat circular velocity curves, spheroids tend to be denser and to have declining V_c curves.

We show the ϵ_j distribution in the right-hand panels of Fig. 1 for three simulated galaxies, chosen to illustrate three representative cases. The top panel corresponds to a galaxy where most stars are in coplanar, nearly circular orbits, hence the sharply-peaked distribution near $\epsilon_j = 1$. The bottom panel corresponds to a spheroidal galaxy where ordered rotation plays little role; the ϵ_j distribution is broad and centered around zero. The middle panel corresponds to an intermediate case, where a non-rotating bulge of stars is surrounded by a well-defined thin disk. A simple quantitative measure of morphology can therefore be constructed by the fraction of stars with circularities exceeding a fixed fiducial value, such as $f(\epsilon_j > 0.5)$.

Although conceptually simple, ϵ_j distributions are not easy to relate to observation, so a simpler quantitative measure of morphology is desirable. One alternative is the fraction of kinetic energy invested in ordered rotation,

$$\kappa_{\rm rot} = \frac{K_{\rm rot}}{K} = \frac{1}{K}\sum \frac{1}{2} m \left(\frac{j_z}{R}\right)^2. \qquad (1)$$

$\kappa_{\rm rot} \sim 1$ for disks with perfect circular motions, and is $\ll 1$ for non-rotating systems. As Fig. 1 makes clear, $\kappa_{\rm rot}$ correlates ex-

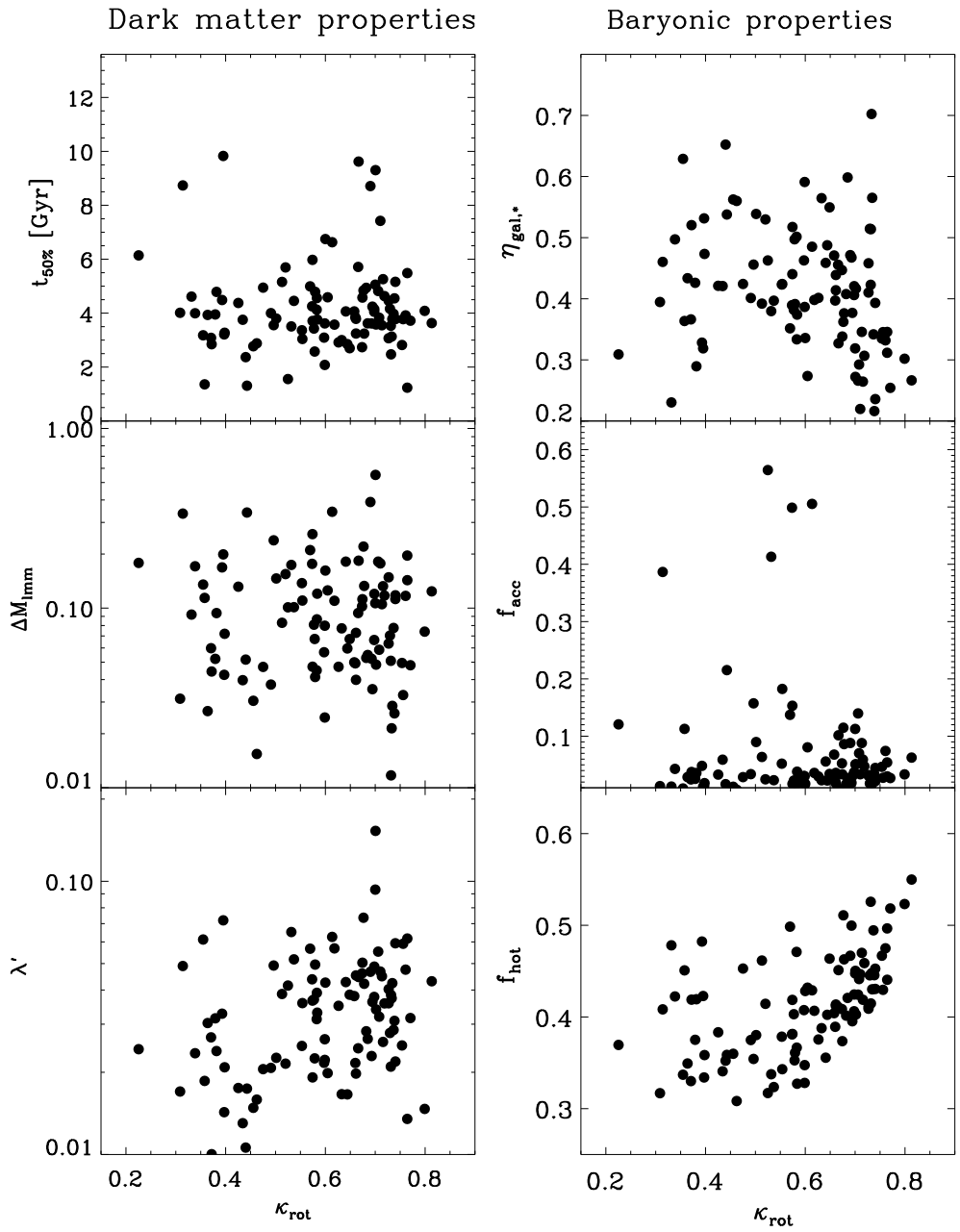

Figure 4. The kinematic morphology parameter, $\kappa_{\rm rot}$, versus a number of parameters characterizing the properties and assembly history of each galaxy and its surrounding halo. On the left, from top to bottom, $t_{50\%}$ is the half-mass halo formation time, in Gyrs; $\Delta M_{\rm lmm}$ is the maximum fraction of the final halo mass assembled in the single largest merger event after $z = 3$; and λ' is the dimensionless rotation parameter (eq. 2). On the right, the galaxy formation "efficiency", $\eta_{\rm gal,*} = M_{\rm gal}/(f_{\rm bar} M_{200})$; $f_{\rm acc}$ is the fraction of *accreted* stars (i.e., stars formed in galaxy progenitors other than the main one) and $f_{\rm hot}$ is the fraction of stars born out of gas that went through the "hot phase" (i.e., $T_{\rm max} > 10^{5.5}$ K). Correlation coefficients for each panel are given in Table 2. See text for further details.

tremely well with the fraction of stars with $\epsilon > 0.5$. In what follows, we shall use $\kappa_{\rm rot}$ to rank galaxies according to the importance of their rotationally-supported components.

For convenience, we shall hereafter refer to galaxies with $\kappa_{\rm rot} < 0.5$ and $\kappa_{\rm rot} > 0.7$ as spheroid- or disk-dominated, respectively. The first group makes up $\sim 25\%$ of the sample; the second group comprises another $\sim 30\%$. The remainder consist of intermediate types where both rotation and velocity dispersion play a comparable structural role. It is important to note that our sample contains galaxies spanning a wide range in $\kappa_{\rm rot}$, from "pure disk" systems with a negligible fraction of stars in counter-rotating orbits (i.e., $j_z < 0$) to spheroids with little trace of rotational support.

3.2 Examples of galaxy morphologies

Fig. 2 shows four examples chosen to illustrate the structure of galaxies with various values of $\kappa_{\rm rot}$. The panels show edge-on and face-on projections of each galaxy, colored by stellar surface mass density on a logarithmic scale. Fig. 3 shows circular velocity profiles and (face-on) stellar surface density profiles. The degree of rotational support increases from left to right: the leftmost and rightmost are spheroid- and disk-dominated systems, respectively, while the two middle ones are intermediate-type objects. Labels in each panel indicate, for each galaxy, the stellar mass within the radius, $r_{\rm gal} = 0.15\, r_{200}$, used to define the central galaxy. Table 1 lists some physical parameters of galaxies A-D.

Figs. 2 and 3, together with Table 1, show that simulated galaxies have several properties in common with nearby ellipticals and spirals. Spheroid-dominated galaxies are gas-poor, dense stellar systems with declining circular velocity curves, whereas disk-dominated galaxies are richer in gas, more spatially extended, and have nearly-flat circular velocity curves. Interestingly, from the point of view of surface density profiles, spheroids are single-component systems well approximated by de Vaucouleurs' $R^{1/4}$ law (dashed magenta lines in the bottom panels of Fig. 3). Disk-dominated systems, on the other hand, have more complex profiles, with a central $R^{1/4}$ spheroid surrounded by an exponential component that increases in importance in step with $\kappa_{\rm rot}$. Like most spirals, they are well approximated by the sum of a de Vaucouleurs' spheroid (dashed magenta lines) and an exponential law (dashed cyan lines).

As discussed in detail by McCarthy et al (in preparation), these similarities with observation actually extend to quantitative comparisons with observed scaling laws, such as the Tully-Fisher relation or the Fundamental Plane. The agreement between simulated galaxies and observation is encouraging, and suggests that the origin of the morphological diversity of simulated galaxies can provide insight into what determines the relative importance of disks and spheroids in real galaxies.

A few caveats should also be mentioned. A wide variety of morphological types does not automatically guarantee reproducing the right morphological mix of galaxies in this mass range. Indeed, a casual inspection suggests that spheroids might be over-represented in our sample. However, because most morphological classifications are based on photometric data, exploring this issue in detail would require synthesizing "observations" of the simulated galaxies in various bands and analyzing them in the same way as observed samples, which is beyond the scope of this work. Moreover, as discussed in Crain et al. (2009), the GIMIC galaxy stellar mass function differs substantially from the observed one, implying that such exercise would be inconclusive, regardless of its results. Our main goal is thus not to test the viability of the particular star formation/feedback implementation adopted in GIMIC, but rather to learn about the various mechanisms responsible for the origin and relative importance of rotationally-supported versus dispersion-supported stellar components in a galaxy.

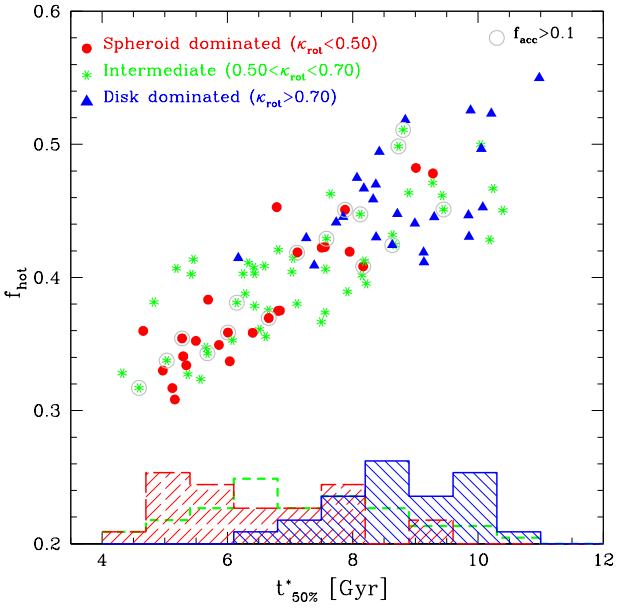

Figure 5. The fraction of stars born from gas that went through the "hot phase" (i.e., $T_{\rm max} > 10^{5.5}$ K) versus the median formation time of stars in the galaxy, $t^*_{50\%,}$. Symbols encircled in grey correspond to systems where more than 10% of stars were accreted in merger events. Each galaxy is color coded according to its morphology: red dots, green asterisks and blue triangles correspond to spheroid-dominated, intermediate, and disk-dominated systems, respectively, as labeled by the $\kappa_{\rm rot}$ parameter. Histograms show the distribution of median formation time for each of these three groups. The tight correlation between $f_{\rm hot}$ and $t^*_{50\%}$ suggest that gas able to reach the "hot phase" take longer to accrete and to be transformed into stars that gas accreted "cold". Late gas accretion clearly favors the assembly of stellar disks.

4 THE ORIGIN OF SIMULATED GALAXY MORPHOLOGIES

4.1 Dependence on dark halo properties

As discussed in Sec. 1, stellar disks are expected to form at the centers of halos with quiet recent accretion histories and high angular momentum. Halos that have been relatively undisturbed by recent major mergers tend to form earlier, so we may also expect stellar disks to inhabit halos with early formation times.

We explore this in Fig. 4, where the left panels show the dependence of $\kappa_{\rm rot}$ on (i) the halo formation time, $t_{50\%}$ (when the most massive halo progenitor reaches half the final halo mass); on (ii) the fraction of halo mass accreted in the single largest merger after $z = 3$, $\Delta M_{\rm lmm}$, and on (iii) the dimensionless rotation parameter,

$$\lambda' = \frac{1}{\sqrt{2}} \frac{J}{M_{200} V_{200} r_{200}}, \qquad (2)$$

where J is the total angular momentum of the halo (Bullock et al. 2001).

None of these parameters correlates strongly with galaxy morphology (see Table 2). Disks form in halos with low and high spin parameter; in halos that collapse early and late, and even in halos that have accreted a substantial amount of mass in merger events. The same applies to spheroids, except perhaps for a weak tendency to prefer halos with slightly lower-than-average λ'.

Fig. 4 also shows that major mergers are uncommon during

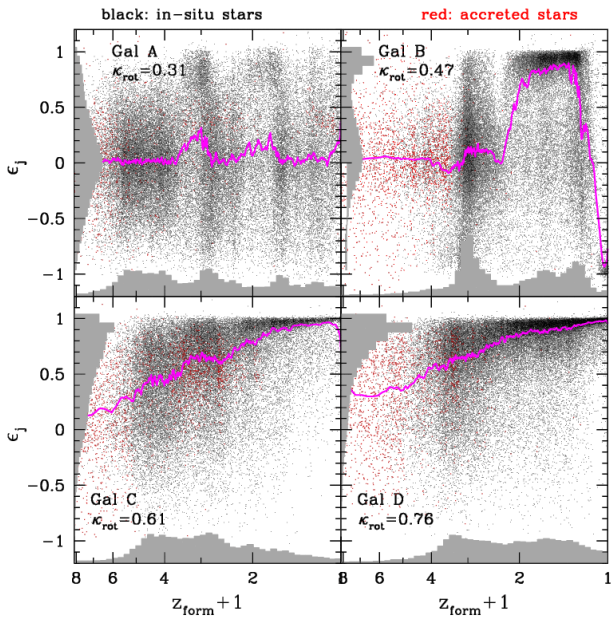

Figure 6. Formation time of stars (expressed in terms of redshift) versus the circularity parameter, ϵ_j, measured at $z = 0$, for the four galaxies illustrated in Fig. 2. Stars formed in the main progenitor (in situ) are shown in black, accreted stars in red. The magenta curve tracks the median circularity as a function of formation time. The two spheroid-dominated galaxies show signs of episodic star formation events that lead to the presence, at $z = 0$, of stellar populations with distinct angular momentum properties. Disks, on the other hand, tend to form more gradually over time and to be dominated by a single population with coherently-aligned angular momentum.

the formation of halos in the narrow mass range considered here; $0.5 < M_{200}/10^{12}\,h^{-1}\,M_\odot < 1.5$. Most systems have accreted less than 20% of their final mass in a single merger since $z = 3$, and these events seem unrelated to the morphology of the central galaxy at $z = 0$.

Finally, morphology also seems unrelated to the fraction of baryons within the virial radius that collects to form the galaxy. This is illustrated in the top-right panel of Fig. 4, where we plot $\kappa_{\rm rot}$ vs the galaxy formation "efficiency" parameter, $\eta_{\rm gal,*} = M_{gal,*}/(f_{\rm bar}\,M_{200})$, where $f_{\rm bar} = \Omega_b/\Omega_m = 0.175$ is the universal baryon fraction. Although we consider halos in a narrow mass range, the efficiency of galaxy formation varies from 20% to 70% (with an average of $\langle\eta_{\rm gal,*}\rangle = 40\%$) and appears to have little influence on the morphology of the central galaxy [2] although there is a weak tendency for disky objects to prefer lower values of $\eta_{\rm gal,*}$.

Thus, contrary to simple expectations, spheroids *can* form in quiescent halos, and disks *can* form in halos of scant angular momentum content. Simple predictions of the morphology of a galaxy based on the properties and assembly history of its surrounding dark halo will thus often be wrong.

[2] We note that abundance matching models (see, e.g., Moster et al. 2010; Guo et al. 2010) demand an even lower galaxy formation efficiency to match the galaxy stellar mass function, which would weaken even further the link between the properties of a central galaxy and that of its surrounding halo.

4.2 Dependence on galaxy history

Galaxy mergers can still in principle play a role in determining morphology, if their importance is underestimated by the *halo* merger parameter $\Delta M_{\rm lmm}$. Indeed, galaxies take longer to merge than halos do, and, due to the large scatter in galaxy formation efficiency, the mass ratio of galaxy mergers may differ substantially from that of their surrounding halos.

We examine the importance of accretion on morphology more explicitly in the middle-right panel of Fig. 4, where we plot $\kappa_{\rm rot}$ vs $f_{\rm acc}$, the fraction of stars *accreted* by the galaxy; i.e., those formed in systems *other* than the main progenitor of the galaxy. This is a direct measure of the importance of accretion events in the build-up of the galaxy. Two points are worth noting here: most galaxies form the majority ($> 90\%$) of their stars *in-situ*, and there is no correlation between $\kappa_{\rm rot}$ and $f_{\rm acc}$. The accreted fraction exceeds 25% in only 5 of our 100 simulated galaxies; overall, accretion events just seem to bring in too few stars to play a significant role in the morphology of our simulated galaxies.

An interesting clue is provided by the thermodynamic history of the gas before it is transformed into stars. This may be estimated simply by tracking every stellar particle back in time and by recording the maximum temperature, $T_{\rm max}$, reached before the particle accretes into the galaxy and becomes eligible for star formation. If $T_{\rm max}$ exceeds $10^{5.5}$ K, then in all likelihood it was accreted by gradual cooling from a shock-heated, nearly hydrostatic gas corona (see, e.g., Crain et al. 2010; van de Voort et al. 2011).

The fraction of stars, $f_{\rm hot}$, whose parent gas particles went through this phase correlates well with $\kappa_{\rm rot}$, indicating that accretion of gas from the "hot phase" favours the formation of disks (see bottom-right panel of Fig. 4). No disk-dominated galaxy (i.e. $\kappa_{\rm rot} > 0.7$) forms unless $f_{\rm hot}$ exceeds 40%. This is intriguing, since it runs counter recent proposals that "cold flows", i.e., gas that gets accreted directly into the galaxy without going through the hot phase, might promote the formation of extended disks (e.g., Kereš et al. 2005; Dekel et al. 2009; Brooks et al. 2009). If anything, our simulations suggest the opposite; the majority of stars in spheroid-dominated galaxies originate in gas that accretes cold.

One reason for this result is illustrated in Fig. 5, which shows that there is a tight correlation between the fraction of stars born from gas that cooled from a hot corona and the median formation time of stars in a galaxy, $t^*_{50\%}$. Heating gas to a hot corona before cooling delays its accretion and favors the late assembly of a galaxy: the larger $f_{\rm hot}$ the later stars form. Enhancing recent star formation promotes the formation of disks and facilitates their survival until the present. This scenario, although appealing, seems incomplete, given the presence of several spheroid-dominated systems that form despite high $f_{\rm hot}$, late $t^*_{50\%}$, and in the absence of significant merger activity.

4.3 Dependence on spin alignment

Our results so far suggest that the morphology of GIMIC galaxies is linked largely to internal mechanisms operating in individual galaxies rather than to accretion-driven transformations. This has been anticipated by semi-analytic models of galaxy formation, where secular evolution driven by "disk instabilities", is thought to be an important formation path for spheroids. These instabilities are assumed to be triggered when the self-gravity of a disk

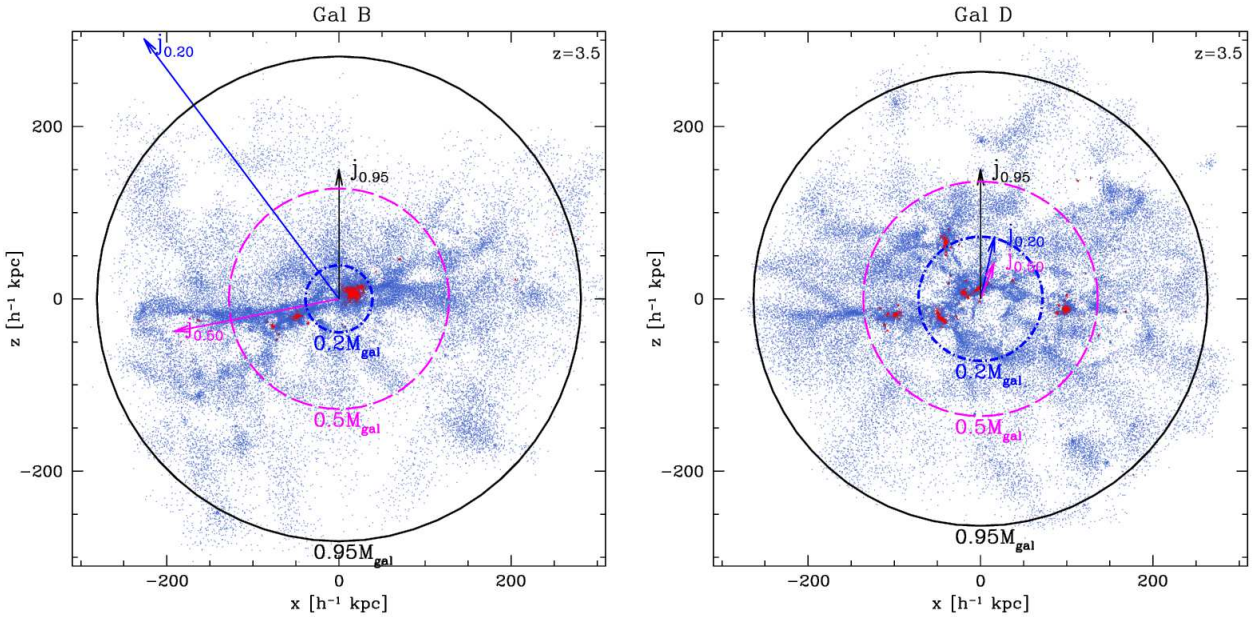

Figure 7. Projected particle distribution near turnaround time, $z = 3.5$, of baryons that collapse to form, at $z = 0$, galaxies B and D shown in Fig. 2. Stars already formed are shown in red, particles still in gaseous form in blue. Box sizes are in physical units. Concentric circles enclose 20%, 50%, and 95% of the mass, and arrows indicate the angular momentum of all material enclosed within each radius. Arrow lengths are normalized to the total value, which defines the z axis of the projection. Each panel is normalized separately, so that $\mathbf{j}_{0.95}$ has equal length in both. Note the misalignment of the angular momentum of various parts of the system for the spheroid-dominated galaxy B. Angular momentum is more coherently acquired in the case of the disk-dominated galaxy D.

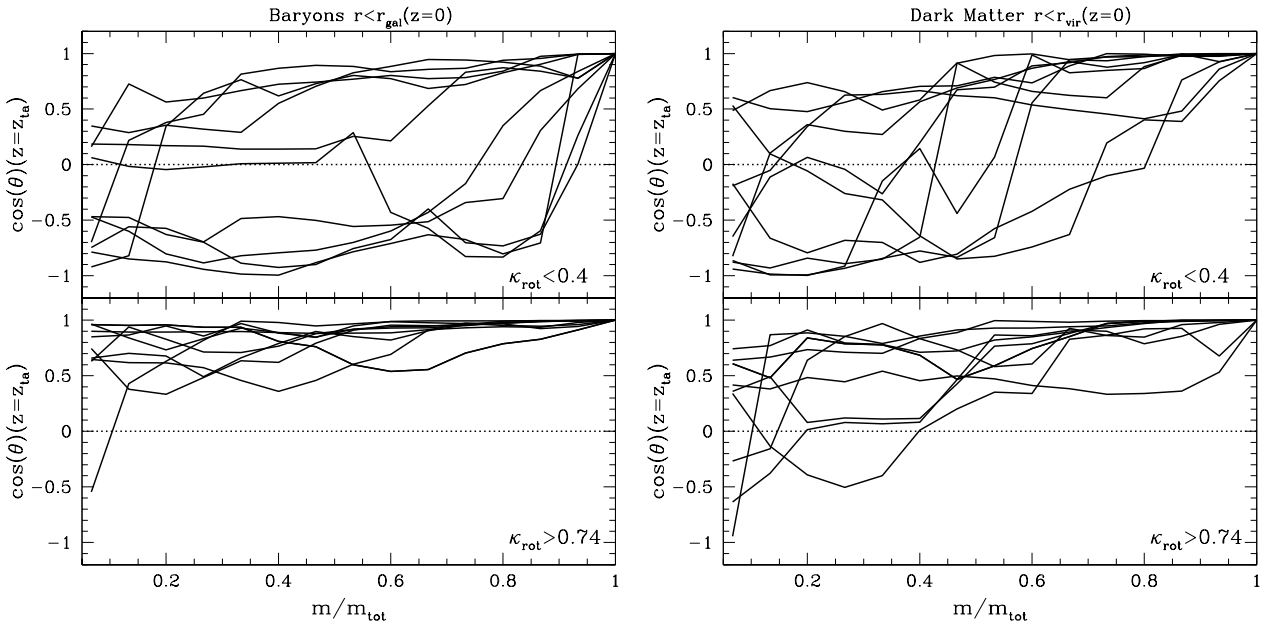

Figure 8. Angle between the angular momentum enclosed within a given mass fraction, $m/m_{\rm tot}$, and the total spin of the system measured at the time of maximum expansion (turnaround) for twenty galaxies in our sample: the ten systems with highest and lowest values of $\kappa_{\rm rot}$ at $z = 0$ and $f_{\rm acc} < 0.1$, respectively. The restriction in $f_{\rm acc}$ is included in order to focus on systems unaffected by merger events. By definition, all curves approach unity as $m \to m_{\rm tot}$. Panels on the left correspond to all baryons within the galaxy radius, $r_{\rm gal}$, at $z = 0$; those on the right to dark matter halo particles that are within r_{200} at $z = 0$. Note the strong misalignments between different parts of the system for galaxies that are spheroid-dominated at $z = 0$, and the smooth alignment characteristic of the turnaround configuration of systems destined to become disks.

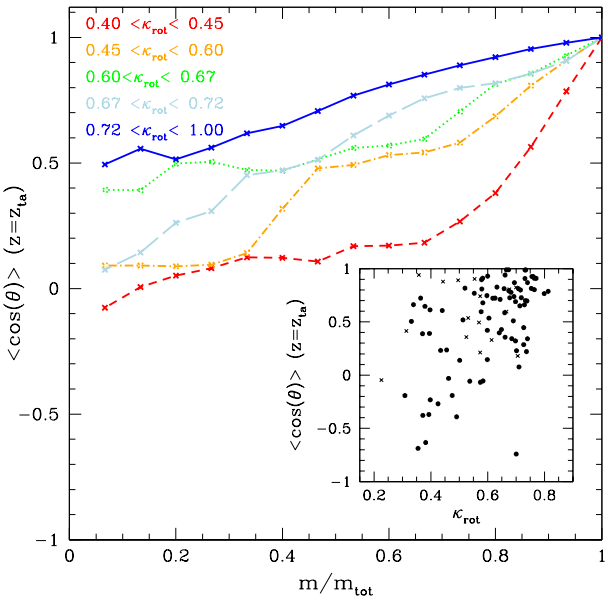

Figure 9. Same as left-hand panel of Fig. 8, but averaged over all galaxies grouped in bins of $\kappa_{\rm rot}$ (at $z = 0$), as labeled. Note that the more disk-dominated a galaxy is at present, the more coherently aligned the spin is at the time of turnaround. The inset panel shows $\langle\cos(\theta)\rangle$ for individual systems, averaged over all mass shells at turnaround, as a function of $\kappa_{\rm rot}$. Galaxies where accretion events have played a minor role, i.e., $f_{\rm acc} < 0.1$, are shown with solid circles, the rest with crosses.

exceeds a particular threshold. For fixed halo mass, as in our sample, this should lead to noticeable correlations between the mass of the galaxy and the importance of the spheroid. However, as we discussed above, no such correlation is apparent.

Recalling the relation between $f_{\rm hot}$, $t^*_{50\%}$, and $\kappa_{\rm rot}$, we look at the star formation history for further clues. Fig. 6 plots the formation redshift, $z_{\rm form}$, of stars in the four galaxies shown in Fig. 2 versus the "circularity" parameter, ϵ_j, measured at $z = 0$. Points in black correspond to stars formed *in-situ* (i.e., within the main progenitor) while those in red are accreted stars.

This figure shows that, as expected, star formation proceeds gradually in disk-dominated systems. In spheroids, however, stars form in separate episodes that leave behind stellar "populations" of different ages and distinct angular momenta. Since most stars form *in-situ*, these populations in galaxies A and B are likely caused by gas accretion events where the net angular momentum of one event is misaligned with the others. On the other hand, disks tend to form out of accreted gas that shares a common angular momentum direction.

These considerations suggest that the final morphology of a galaxy is imprinted early on, since the spin of the material destined to form a galaxy is acquired at the time of maximum expansion and changes little in the absence of merging (see, e.g., White 1984; Navarro et al. 2004). We illustrate this by studying the angular momentum of galaxies B and D at $z = 3.5$, which roughly corresponds to the time of turnaround of both systems. Fig. 7 shows the spatial distribution of all baryons that will end up within $r_{\rm gal}$ at $z = 0$. Net angular momentum is acquired through the interplay between the inertia tensor of the mass distribution and the shear tensor due to the large-scale distribution of surrounding matter, so that the direction of the acquired spin usually aligns with the *intermediate axis* of the mass distribution (Catelan & Theuns 1996; Porciani et al. 2002a,b; Navarro et al. 2004). For highly non-uniform spatial distributions, where the principal axes of the inertia tensor can change direction abruptly, this effect may cause the net angular momentum of different parts of the system to flip and misalign.

We see from Fig. 7 that this is indeed the case for galaxy B. Here the arrows indicate the direction and magnitude, at $z = 3.5$, of the specific angular momentum of the inner 20%, 50% and 95% of the baryons that end up in the galaxy at $z = 0$. The length of the arrows is normalized to the total, which is chosen by construction to coincide with the z axis of the projection. The angular momenta of different parts of the system are clearly misaligned: the angle between $\mathbf{j}_{0.2}$ and $\mathbf{j}_{0.5}$ is 85 degrees, and that between $\mathbf{j}_{0.5}$ and $\mathbf{j}_{0.95}$ is ~ 100 degrees. Since gas further out in Fig. 7 takes longer to accrete, newly assembled material will be misaligned with the rest, leading to the formation of distinct populations of stars (shown in Fig. 6) that will tend to destabilize any existing disk and to cancel out the net angular momentum of the system; leaving in place a slowly-rotating stellar spheroid.

On the other hand, the spins of different parts of the system are very well aligned in the case of the disk-dominated galaxy D, as shown in Fig. 7. This coherence in the angular momentum at turnaround allows newly accreted material to settle into a stable disk where star formation can proceed gradually and smoothly.

We show in Fig. 8 that this result applies to the majority of spheroid- and disk-dominated galaxies in our sample. Here we plot, for the ten galaxies with highest and lowest values of $\kappa_{\rm rot}$ where accretion has played a minor role ($f_{\rm acc} < 0.1$), the cosine of the angle θ between the angular momentum of a given enclosed mass fraction $m/m_{\rm tot}$ and the direction of the total spin of the system. By construction, each curve in Fig. 8 is constrained to approach unity as the enclosed mass approaches $m_{\rm tot}$.

It is clear from this figure that different regions of systems destined to form spheroid-dominated galaxies have, at turnaround, large misalignments in their acquired spin. Indeed, in many cases the inner regions counterrotate (i.e., $\cos(\theta) < 0$) relative to the outer regions of the system. This is not the case for systems that become disk-dominated which, in general, show coherence in the alignment of the spin axis. In these cases, the enclosed specific angular momentum increases roughly linearly with enclosed mass fraction. As Fig. 9 shows, the same result applies to all galaxies in our sample: despite the large scatter, on average, the degree of alignment at turnaround increases gradually with the importance of the disk component in the morphology of a galaxy at $z = 0$.

The right panels in Fig. 8 show that a similar assessment applies to the dark matter halo surrounding these galaxies. The halos of spheroids also show, at turnaround, stronger misalignments than the halos that host disk galaxies at $z = 0$. This is encouraging, since it implies that it might be possible to use the angular momentum properties of a dark matter halo at turnaround to "predict" the morphology of its central galaxy at $z = 0$. We emphasize, however, that the trends we highlight here, although well defined, are relatively weak, so the correspondence between early halo properties and final galaxy morphology is likely to apply statistically rather than to individual systems.

Quantitatively, the dependence of present day morphology on spin alignment at turnaround is shown in the inset panel of Fig. 9. Here we show, for each individual system, $\kappa_{\rm rot}$ versus the average cosine of the angle, at turnaround, between the angular momen-

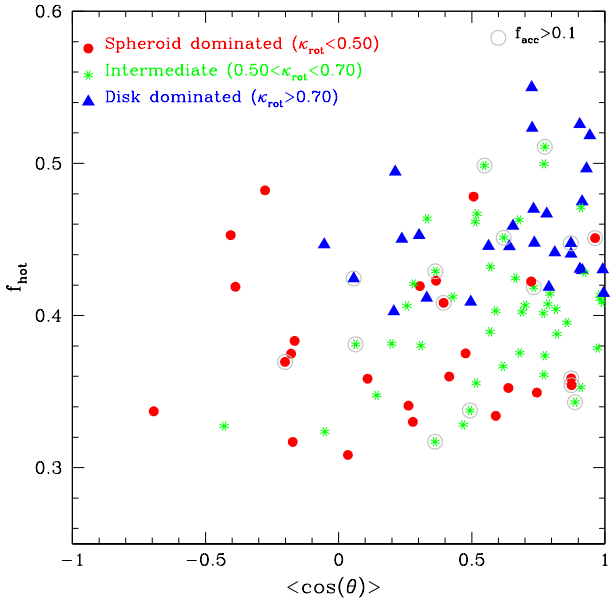

Figure 10. Fraction of stars born from gas accreted from the "hot phase" as a function of the alignment parameter $\langle\cos(\theta)\rangle$ at the time of turnaround. Color-coding is the same as in Fig. 5. Note that, in general, disk-dominated, spheroid-dominated, and intermediate systems occupy different regions in this diagram. See text for further discussion.

tum enclosed by different mass shells and the total. The trend is clear: systems with better-aligned spins at turnaround tend to be more disk-dominated at present. The trend is even stronger when considering only systems where mergers have played a minor role ($f_{\rm acc} < 0.1$, solid points). The correlation coefficient is $r_s = 0.49$ (with significance $\Delta \sim 2 \times 10^{-6}$) and confirms our earlier conclusion that significant misalignment in the distribution of angular momentum can lead to the formation of spheroid-dominated systems in the absence of significant merger events.

4.4 Spin alignment vs mode of accretion

The results of the above subsections suggest that there are (at least) two mechanisms responsible for the morphology of GIMIC galaxies: the alignment of the spin acquired by various parts of a galaxy and the mode of gas accretion. Fig. 10 shows that these two effects are approximately independent of each other: there is no obvious correlation between the fraction of gas accreted from the hot phase and the alignment parameter $\langle\cos(\theta)\rangle$. However, disk-dominated systems (blue triangles) separate from spheroid-dominated ones (red circles) fairly neatly in this plane, suggesting that $\kappa_{\rm rot}$ is determined by a combination of the two mechanisms.

Large $f_{\rm hot}$ favors disk formation: gas shock-heated into a nearly-hydrostatic corona of hot gas is forced to homogenize its rotational properties before accretion, providing the forming galaxy with a gradual supply of gas that shares the same spin axis (see, e.g., Brook et al. 2012). Disk-dominated systems then form when $f_{\rm hot}$ is large, unless the spin misalignments are large enough to disrupt them: no disk-dominated system forms when $\langle\cos(\theta)\rangle < 0$, even for relatively large values of $f_{\rm hot}$.

Spheroids, on the other hand, form primarily when cold gas accretion prevails ($f_{\rm hot} < 0.4$): gas that flows along distinct filaments cannot interact hydrodynamically before accretion and will often have misaligned net spins. Each accretion event then results in the formation of a "population" of misaligned stars that will tend to destabilize any existing disk and to cancel out the net angular momentum of the system, leaving in place a slowly-rotating stellar spheroid. Intermediate systems, in general, result when the deleterious effects on stellar disks of cold accretion events are mitigated by well-aligned spins.

In other words, spheroid-dominated galaxies in our sample do not originate from disk instabilities triggered by self-gravity, as envisioned by semi-analytic models, but rather by the accretion of gas that settles on off-axis orbits relative to earlier accreted material. This has been seen in earlier work (e.g., Brook et al. 2008; Scannapieco et al. 2009), and might be related to sudden changes in the orientation of the dark matter halos as discussed in Bett & Frenk (2011). Its relevance to the formation of the whole class of spheroidal galaxies, in the absence of merging, has not yet been recognized and emphasized.

We hasten to add that the importance of this mechanism for the formation of spheroids might depend on halo mass, and that we explore only a narrow range here: $0.5 < M_{200}/10^{12}\,h^{-1}M_\odot < 1.5$. This caveat might be particularly relevant in the case of the most massive spheroids, where merging likely plays a more important role (e.g. Parry et al. 2009; De Lucia et al. 2011; Feldmann et al. 2010). Caution must also be exercised when extrapolating the link between morphology and the fraction of stars born from hot accretion. Disk-dominated galaxies might still form out of cold accretion if, for example, the most recent episode of accretion supplies most of the mass of the system. Repeated cold accretion events may hinder disk formation, but a single major event may very well facilitate it.

5 SUMMARY

We use gasdynamical cosmological simulations of galaxy formation to study the origin of different galaxy morphologies in the ΛCDM cosmogony at redshift $z = 0$. The GIMIC simulation series covers a large volume and has a resolution high enough to study the structure and kinematics of the stellar components of 100 central galaxies in Milky Way-sized halos. We focus our analysis on the origin of galaxy morphology, somewhat narrowly defined as the relative importance of rotational support vs velocity-dispersion support (the disk-to-spheroid ratio) in the structure of the galaxy. Our main results may be summarized as follows:

- The simulated galaxies span a wide range of morphological types, from rotation-free spheroids to almost pure disk galaxies where fewer than 5% of all stars are in counterrotating orbits. Disks have roughly exponential stellar surface density profiles and flat rotation curves, whereas spheroids are dense stellar systems that can be approximated by de Vaucouleurs' $R^{1/4}$ profiles. The resemblance with real galaxies suggests that it should be possible to gain insight into the origin of galaxy morphology by studying the mechanisms responsible for the relative importance of disks and spheroids in GIMIC galaxies.
- The morphology of simulated galaxies seems mostly unrelated to the spin or assembly history of their surrounding dark matter halos. Most stars form *in-situ* and comprise on average about $\sim 40\%$ of all available baryons in the halo. Most baryons in a halo therefore end up not making part of the central galaxy, which helps to explain the weak correlation between the properties of halos and

those of central galaxies. Contrary to simple expectations, disks form in halos with low and high angular momenta, and spheroids form even in galaxies where most stars form *in-situ*, suggesting a formation path for spheroids that does not rely on merging.

- The star formation history provides an interesting clue to the origin of morphology. Disks tend to have young stars, and to form gradually over long periods of time. This is because gradual cooling from a hot corona delays the accretion of gas and promotes late star formation.
- Star formation in spheroids proceeds episodically, leaving behind populations of stars of similar age but distinct kinematics. These populations originate from the accretion of gas whose angular momentum is misaligned relative to that of earlier-accreted material. The misalignment destabilizes any pre-existing disk, prompts the rapid transformation of gas into stars, and reduces the net rotational support of the system.
- Since angular momentum is largely acquired at the time of maximum expansion of the material destined to form a galaxy, a good indicator of morphology at $z = 0$ is the coherence in the alignment of the net spin of various parts of the system at the time of turnaround. Spheroid-dominated galaxies form in systems where misalignments are substantial whereas disks form in systems where the angular momentum of all mass shells is roughly aligned.
- The final morphology of a galaxy results from the combined effects of spin alignment and of hot/cold gas accretion. Disk-dominated objects are made of stars formed predominantly *in situ*, and avoid systems where most baryons were accreted cold, or those where spin misalignments are extreme. On the other hand, direct filamentary accretion of cold gas, especially when accompanied by substantial spin misalignments, favours the formation of slowly-rotating spheroids, which may thus form even in the absence of mergers.

Our results suggest a new scenario for the origin of $\sim L_*$ stellar spheroids that does not rely on merging. This scenario, once developed more thoroughly, should offer a number of predictions falsifiable by observation. For example, the episodic nature of star formation in spheroids envisioned here is expected to leave behind overlapping populations of stars of distinct age, kinematics, and, possibly, metallicity) that survive to the present because of the paucity of mergers. We plan to explore the observational signatures of these populations in future work.

The scenario we propose here also offers clues to the origin of pure disk galaxies. A number of our simulated galaxies have virtually no "classical" spheroid, with fewer than 5% of their stars in counterrotating orbits. These galaxies form either in systems where spin alignment is extraordinarily coherent or where most of the baryons in the galaxy get accreted late from a hot corona. Although at this time limited numerical resolution precludes a more detailed study, we plan to use these clues to resimulate some of these systems at higher resolution with the goal of shedding light into the origin of bulgeless galaxies.

We emphasize that, although coherent spin alignment at early times is clearly an important clue, it should be considered as one ingredient of the complex process that determines the morphology of a galaxy. Strong feedback, for example, may expel baryons from galaxies and cycle them through a hot corona before they get re-accreted and turned into stars, potentially erasing the spin alignment dependence at turnaround we report here. Furthermore, aligned spins in the accreting gas might not be enough to ensure the survival of a stellar disk, especially if the dark matter halo is strongly triaxial and its principal axes are not coincident with the disk. Finally, although mergers are rare in the mass range we explore here, they likely play a more important role in the formation of more massive spheroids. Until simulations can reproduce not only the properties of individual systems, but the full statistical distribution of galaxy morphologies and their dependence on mass and environment, it is likely that a full understanding of the origin of galaxy morphology will remain beyond reach.

Table 1. Summary of main properties for Gal A-D in Fig. 2 and 3. Rows correspond to the virial mass M_{200}; galactic mass in stars $M_{\rm str}$; gas $M_{\rm gas}$ and gas fraction $f_{\rm gas}$; peak circular velocity $V_{\rm max}$; the circular velocity measured at the galactic radius $V_c(r = r_{\rm gal})$; the degree of rotational support $\kappa_{\rm rot}$; and the fraction of the stars in counter-rotating orbits f_c.

Property	Gal A	Gal B	Gal C	Gal D
$M_{200}[10^{12}h^{-1}M_\odot]$	1.18	0.98	0.77	1.04
$M_{\rm str}(r < r_{\rm gal})[10^{10}h^{-1}M_\odot]$	8.98	7.25	5.42	6.31
$M_{\rm gas}(r < r_{\rm gal})[10^{10}h^{-1}M_\odot]$	0.51	0.72	1.00	1.86
$f_{\rm gas}(M_{\rm gas}/(M_{\rm gas} + M_{\rm str}))$	0.05	0.09	0.15	0.23
$V_{\rm max}$ [km/s]	471	383	300	280
$V_c(r = r_{\rm gal})$ [km/s]	187	172	160	178
$\kappa_{\rm rot}$	0.31	0.47	0.61	0.76
f_c	0.48	0.33	0.12	0.06

Table 2. Spearman rank correlation coefficients, r_s, between $\kappa_{\rm rot}$ and the halo/galaxy properties shown in Figs. 4 and 9. The second column shows the two-sided significance of its deviation from zero, as computed by the IDL subroutine `r-correlate`: smaller values indicate more significant correlations.

Property	r_s	Δ
$t_{50\%}$	0.05	0.60
$\Delta_{\rm lmm}$	-0.06	0.57
λ'	0.29	2.8×10^{-3}
$\eta_{gal,*}$	-0.30	1.9×10^{-3}
$f_{\rm acc}$	0.06	0.55
$f_{\rm hot}$	0.55	1.6×10^{-9}
$< \cos(\theta) >$	0.41	2.0×10^{-5}

ACKNOWLEDGEMENTS

We thank the anonymous referee for a prompt and useful report. We thank Ian McCarthy for his contribution to the simulations used in this work, which were run at the Darwin HPC of Cambridge University. LVS is grateful for financial support from the CosmoComp/Marie Curie network. CSF acknowledges a Royal Society Wolfson research merit award and ERC Advanced Investigator grant COSMIWAY. This work was supported in part by an STFC rolling grant to the ICC.

REFERENCES

Abadi M. G., Navarro J. F., Steinmetz M., Eke V. R., 2003, ApJ, 591, 499
Agertz O., Teyssier R., Moore B., 2011, MNRAS, 410, 1391
Bett P. E., Frenk C. S., 2011, ArXiv e-prints

Bournaud F., Chapon D., Teyssier R., Powell L. C., Elmegreen B. G., Elmegreen D. M., Duc P.-A., Contini T., Epinat B., Shapiro K. L., 2011, ApJ, 730, 4
Bower R. G., Benson A. J., Malbon R., Helly J. C., Frenk C. S., Baugh C. M., Cole S., Lacey C. G., 2006, MNRAS, p. 659
Brook C. B., Governato F., Quinn T., Wadsley J., Brooks A. M., Willman B., Stilp A., Jonsson P., 2008, ApJ, 689, 678
Brook C. B., Governato F., Roškar R., Stinson G., Brooks A. M., Wadsley J., Quinn T., Gibson B. K., Snaith O., Pilkington K., House E., Pontzen A., 2011, MNRAS, 415, 1051
Brook C. B., Stinson G., Gibson B. K., Roškar R., Wadsley J., Quinn T., 2012, MNRAS, 419, 771
Brooks A. M., Governato F., Quinn T., Brook C. B., Wadsley J., 2009, ApJ, 694, 396
Bullock J. S., Dekel A., Kolatt T. S., Kravtsov A. V., Klypin A. A., Porciani C., Primack J. R., 2001, ApJ, 555, 240
Bundy K., Treu T., Ellis R. S., 2007, ApJL, 665, L5
Catelan P., Theuns T., 1996, MNRAS, 282, 436
Cen R., Chisari N. E., 2011, ApJ, 731, 11
Ceverino D., Klypin A., 2009, ApJ, 695, 292
Chabrier G., 2003, ApJL, 586, L133
Christodoulou D. M., Shlosman I., Tohline J. E., 1995, ApJ, 443, 551
Cole S., Lacey C. G., Baugh C. M., Frenk C. S., 2000, MNRAS, 319, 168
Crain R. A., McCarthy I. G., Frenk C. S., Theuns T., Schaye J., 2010, MNRAS, 407, 1403
Crain R. A., Theuns T., Dalla Vecchia C., Eke V. R., Frenk C. S., Jenkins A., Kay S. T., Peacock J. A., Pearce F. R., Schaye J., Springel V., Thomas P. A., White S. D. M., Wiersma R. P. C., 2009, MNRAS, 399, 1773
Croft R. A. C., Di Matteo T., Springel V., Hernquist L., 2009, MNRAS, 400, 43
Croton D. J., Springel V., White S. D. M., De Lucia G., Frenk C. S., Gao L., Jenkins A., Kauffmann G., Navarro J. F., Yoshida N., 2006, MNRAS, 365, 11
Dalla Vecchia C., Schaye J., 2008, MNRAS, 387, 1431
De Lucia G., Fontanot F., Wilman D., Monaco P., 2011, MNRAS, 414, 1439
Dekel A., Birnboim Y., 2006, MNRAS, 368, 2
Dekel A., Sari R., Ceverino D., 2009, ApJ, 703, 785
Dolag K., Borgani S., Murante G., Springel V., 2009, MNRAS, 399, 497
Efstathiou G., Lake G., Negroponte J., 1982, MNRAS, 199, 1069
Eggen O. J., Lynden-Bell D., Sandage A. R., 1962, ApJ, 136, 748
Fall S. M., Efstathiou G., 1980, MNRAS, 193, 189
Feldmann R., Carollo C. M., Mayer L., Renzini A., Lake G., Quinn T., Stinson G. S., Yepes G., 2010, ApJ, 709, 218
Font A. S., McCarthy I. G., Crain R. A., Theuns T., Schaye J., Wiersma R. P. C., Dalla Vecchia C., 2011, MNRAS, 416, 2802
Frenk C. S., White S. D. M., Efstathiou G., Davis M., 1985, Nature, 317, 595
Governato F., Brook C. B., Brooks A. M., Mayer L., Willman B., Jonsson P., Stilp A. M., Pope L., Christensen C., Wadsley J., Quinn T., 2009, MNRAS, 398, 312
Governato F., Willman B., Mayer L., Brooks A., Stinson G., Valenzuela O., Wadsley J., Quinn T., 2007, MNRAS, 374, 1479
Guedes J., Callegari S., Madau P., Mayer L., 2011, ApJ, 742, 76
Guo Q., White S., Li C., Boylan-Kolchin M., 2010, MNRAS, pp 367–376
Haardt F., Madau P., 2001, in D. M. Neumann & J. T. V. Tran ed., Clusters of Galaxies and the High Redshift Universe Observed in X-rays Modelling the UV/X-ray cosmic background with CUBA
Hahn O., Teyssier R., Carollo C. M., 2010, MNRAS, 405, 274
Hopkins P. F., Bundy K., Croton D., Hernquist L., Keres D., Khochfar S., Stewart K., Wetzel A., Younger J. D., 2010, ApJ, 715, 202
Hubble E. P., 1926, ApJ, 64, 321
Kennicutt Jr. R. C., 1989, ApJ, 344, 685
Kennicutt Jr. R. C., 1998, ARA&A, 36, 189
Kereš D., Katz N., Weinberg D. H., Davé R., 2005, MNRAS, 363, 2
Larson R. B., 1974, MNRAS, 166, 585
Larson R. B., 1976, MNRAS, 176, 31
Lotz J. M., Jonsson P., Cox T. J., Croton D., Primack J. R., Somerville R. S., Stewart K., 2011, ApJ, 742, 103
McCarthy I. G., Font A. S., Crain R. A., Deason A. J., Schaye J., Theuns T., 2011, ArXiv e-prints
Meza A., Navarro J. F., Steinmetz M., Eke V. R., 2003, ApJ, 590, 619
Mo H. J., Mao S., White S. D. M., 1998, MNRAS, 295, 319
Moster B. P., Somerville R. S., Maulbetsch C., van den Bosch F. C., Macciò A. V., Naab T., Oser L., 2010, ApJ, 710, 903
Navarro J. F., Frenk C. S., White S. D. M., 1995, MNRAS, 275, 56
Navarro J. F., Hayashi E., Power C., Jenkins A. R., Frenk C. S., White S. D. M., Springel V., Stadel J., Quinn T. R., 2004, MNRAS, 349, 1039
Navarro J. F., Steinmetz M., 1997, ApJ, 478, 13
Oesch P. A., Carollo C. M., Feldmann R., Hahn O., Lilly S. J., Sargent M. T., Scarlata C., 24 coauthors 2010, ApJL, 714, L47
Okamoto T., Eke V. R., Frenk C. S., Jenkins A., 2005, MNRAS, 363, 1299
Parry O. H., Eke V. R., Frenk C. S., 2009, MNRAS, 396, 1972
Partridge R. B., Peebles P. J. E., 1967, ApJ, 147, 868
Piontek F., Steinmetz M., 2011, MNRAS, 410, 2625
Porciani C., Dekel A., Hoffman Y., 2002a, MNRAS, 332, 325
Porciani C., Dekel A., Hoffman Y., 2002b, MNRAS, 332, 339
Power C., Navarro J. F., Jenkins A., Frenk C. S., White S. D. M., Springel V., Stadel J., Quinn T., 2003, MNRAS, 338, 14
Robertson B., Bullock J. S., Cox T. J., Di Matteo T., Hernquist L., Springel V., Yoshida N., 2006, ApJ, 645, 986
Sales L. V., Navarro J. F., Schaye J., Dalla Vecchia C., Springel V., Booth C. M., 2010, MNRAS, 409, 1541
Sales L. V., Navarro J. F., Schaye J., Dalla Vecchia C., Springel V., Haas M. R., Helmi A., 2009, MNRAS, 399, L64
Scannapieco C., Gadotti D. A., Jonsson P., White S. D. M., 2010, MNRAS, 407, L41
Scannapieco C., Tissera P. B., White S. D. M., Springel V., 2008, MNRAS, 389, 1137
Scannapieco C., White S. D. M., Springel V., Tissera P. B., 2009, MNRAS, 396, 696
Schaye J., Dalla Vecchia C., 2008, MNRAS, 383, 1210
Schaye J., Dalla Vecchia C., Booth C. M., Wiersma R. P. C., Theuns T., Haas M. R., Bertone S., Duffy A. R., McCarthy I. G., van de Voort F., 2010, MNRAS, 402, 1536
Somerville R. S., Barden M., Rix H.-W., Bell E. F., Beckwith S. V. W., Borch A., Caldwell J. A. R., Häußler B., Heymans C., Jahnke K., Jogee S., McIntosh D. H., Meisenheimer K., Peng C. Y., Sánchez S. F., Wisotzki L., Wolf C., 2008, ApJ, 672, 776
Springel V., 2005, MNRAS, 364, 1105
Springel V., White S. D. M., Jenkins A., Frenk C. S., Yoshida N., Gao L., Navarro J., Thacker R., Croton D., Helly J., Peacock J. A., Cole S., Thomas P., Couchman H., Evrard A., Colberg J.,

Pearce F., 2005, Nature, 435, 629
Springel V., Yoshida N., White S. D. M., 2001, New Astronomy, 6, 79
Steinmetz M., Navarro J. F., 2002, New Astronomy, 7, 155
Toomre A., 1977, in Tinsley B. M., Larson R. B., eds, Evolution of Galaxies and Stellar Populations Mergers and Some Consequences. p. 401
van de Voort F., Schaye J., Booth C. M., Haas M. R., Dalla Vecchia C., 2011, MNRAS, 414, 2458
Vogelsberger M., Sijacki D., Keres D., Springel V., Hernquist L., 2011, ArXiv e-prints
White S. D. M., 1984, ApJ, 286, 38
White S. D. M., Frenk C. S., 1991, ApJ, 379, 52
White S. D. M., Rees M. J., 1978, MNRAS, 183, 341
Wiersma R. P. C., Schaye J., Smith B. D., 2009, MNRAS, 393, 99
Wiersma R. P. C., Schaye J., Theuns T., Dalla Vecchia C., Tornatore L., 2009, MNRAS, 399, 574